

# Effectiveness of Four Types of WorldView-2/3 Features in Tree Species Identification

Huapeng Liu

## Abstract

Extracting key features from remote sensing imagery for the purpose of identifying tree species holds significant importance. To assess the importance of the newly proposed polygon area index (PAI) and other features in classifying tree species, this research employed WorldView-3/2 (WV-3/2) as the experimental dataset and constructed four distinct feature sets: spectral bands, HSVs (hue, saturation, and value), textures and PAIs. Then, these feature sets and their combinations were utilized, and the random forest method was applied to classify tree species and ascertain the importance of the features involved in the classification process. The experimental results demonstrate that all texture features play a crucial role in the identification of tree species, with eight features being selected. Additionally, numerous HSV features (WV-3: 29, WV-2: 21) and PAI features (WV-3: 7, WV-2: 4) also make significant contributions. However, the spectral bands did not show a notable positive impact, as none were selected. When compared with the use of single-type features, the integration of multiple features from WorldView-3/2 resulted in more effective tree species identification, achieving an overall accuracy of 90.45% for WV-3 and 84.60% for WV-2, surpassing the highest overall accuracy achieved by single-type features, which was 76.64% for WV-3 and 78.27% for WV-2. The experimental results indicate that multi-type features should be used for tree species classification. Additionally, the newly proposed PAI feature demonstrates a positive contribution and is recommended for active use in tree species classification.

**Keywords:** WorldView-3/2, four types of features, tree species identification, effectiveness evaluation, random forest

## 1. Introduction

The use of remote sensing methods for identifying tree species is currently a research hotspot, given its potential to overturn the longstanding reliance on manual fieldwork for tree species investigation. In tree species identification research using remote sensing methods, the spectral bands of remote sensing imagery, along with image features such as texture features, spectral indices and color space features derived from these spectral bands, exhibit characteristics that effectively capture the differences among tree species. Consequently, strategically integrating these diverse feature types has the potential to considerably enhance the accuracy of tree species identification. If it is feasible to clarify the effectiveness of various feature types and their combinations in remote sensing imagery for tree species identification, valuable insights can be gained from the selection and exclusion of image features in

remote sensing-based tree species identification. Therefore, analyzing the utility of various image features in tree species identification holds significant value in enhancing the accuracy and effectiveness of remote sensing-based tree species identification.

In the realm of tree species identification using remote sensing techniques, a diverse array of data sources has proven invaluable. Among these, IKONOS, QuickBird, and WorldView-3/2 (WV-3/2) satellites provide high-resolution imagery, capturing intricate details of the tree canopy and underlying structures (Ghosh and Joshi 2014, Ferreira et al. 2019). Elevation data, obtained through various means such as lidar scanning, provide crucial information on tree heights, which is often a key factor in distinguishing between different species (Naidoo et al. 2012, Hamraz et al. 2019, Shi and Wang 2020). Additionally, the emergence of unmanned aerial vehicles has revolutionized data

collection, enabling the capture of multispectral and hyperspectral data with unprecedented precision (Torabzadeh et al. 2019, Modzelewska et al. 2020). Hyperspectral data, in particular, offers a detailed spectral signature of trees, enabling the identification of subtle differences in leaf chemistry that can be used to classify different species (Zhang et al. 2016, Zhang et al. 2020). The combination of these diverse data sources, especially those incorporating high spatial resolution and tree height information, significantly enhances the accuracy and reliability of tree species classification (Richards and Jia 2008, Kureel et al. 2021).

Focusing on the use of image features in tree species identification, scholars extensively use various image feature types, including image layers of bands, spectral indices, textures, and digital surface models (DSMs) (Wang et al. 2016, Åkerblom et al. 2017, Yu et al. 2017). Beyond the conventional features, some researchers are also pioneering the development of novel image features that cater specifically to the needs of tree species classification (Zhou et al. 2011). My contribution lies in the development of a polygon area index (*PAI*) for tree species identification (Liu 2023a). This index is based on the observation that the area enclosed by each species' spectral curve and the coordinate axes – where the horizontal and vertical axes represent wavelength and reflectance – differs among tree species. Feature layers derived from these area differences can effectively capture the distinctions among tree species. Both their efforts and mine aim to enrich the differentiated information in remote sensing images, capturing the intricacies of tree species from diverse perspectives (Zhou et al. 2011, Liu and An 2020a, Liu 2023a, Liu 2023b). According to research, texture features and DSMs have demonstrated significant potential in mapping tree species, often outperforming other types of features (Liu 2022, Liu 2024). Moreover, the incorporation of these innovative features, such as the *PAI*, has been shown to enhance the accuracy of tree species recognition (Zhou et al. 2011, Liu and An 2020a, Liu 2023a). The use of multi-source data and a vast array of image features in remote sensing imagery serves as a valuable asset in the identification of tree species (Cross et al. 2019, Apostol et al. 2020).

For the temporal phase selection of remote sensing images, the selection of the appropriate temporal phase for tree species classification is crucial. While numerous studies have relied solely on single-phase data for this purpose (Liu et al. 2015, Liu and An 2019), a growing number of scholars have advocated for the utilization of multi-phase data (Pu et al. 2018, Masemola et al. 2019, Shi et al. 2020, Liu 2022). This approach is grounded in the understanding that single-phase data

sources often fall short in highlighting the phenological variations unique to different tree species within the imagery. By incorporating multi-temporal data, researchers are able to capture these phenological differences, which can substantially enhance the accuracy of tree species classification (Han et al. 2019, Immitzer et al. 2019, Liu 2024). Not only does this method compensate for the limitations of single-phase data, but it also provides a more comprehensive understanding of the temporal dynamics of tree species, leading to more informed and precise classification outcomes.

Previously, traditional classifiers such as maximum likelihood classifier (MLC), support vector machines (SVM), and random forests (RF) played a significant role in tree species classification (Lin et al. 2015, Modzelewska et al. 2020, Liu 2023a). MLC offers rapid speed and high accuracy in low-dimensional data, but it suffers from the Hughes phenomenon in higher dimensions (Ghosh and Joshi 2014, Liu 2024). SVM boasts high accuracy and resilience to feature dimensionality, albeit with a lengthy training time. Deep learning methods have shown promise in achieving high accuracy for tree species recognition, yet they also require considerable training time (Kemal et al. 2019, Carvalho et al. 2022, Kwon et al. 2023). Conversely, RF is not affected by feature dimensionality, possesses swift training speed, high classification accuracy, and the ability to rank feature importance. For multispectral data, the choice of classifier depends on the number and complexity of extracted image features. When the number of features is small, MLC may suffice, while for larger feature sets requiring faster processing, RF emerges as a preferred option.

From the literature review, it is evident that in tree species classification, apart from factors like data source, imaging time, and the choice of classifiers, scholars have also devoted significant attention to the selection of crucial image features. In previous studies, we identified the potential significance of hue, saturation, and value (*HSV*) as well as the newly introduced *PAI*, in tree species identification (Liu and An 2019, Liu 2023a). Given that texture features play a crucial role in tree species classification, and spectral bands serve as fundamental data for tree species recognition, I hypothesize that integrating these feature types could be invaluable for tree species identification. In this study, I employed *HSVs*, *PAIs*, texture features, spectral bands, and their combinations to classify tree species. My objective was to evaluate the effectiveness of these features in identifying tree species. This evaluation aims to clarify the performance of several key feature types in tree species identification. I intend to utilize WV-3/2 as the data source to extract *HSVs*, *PAIs*, and

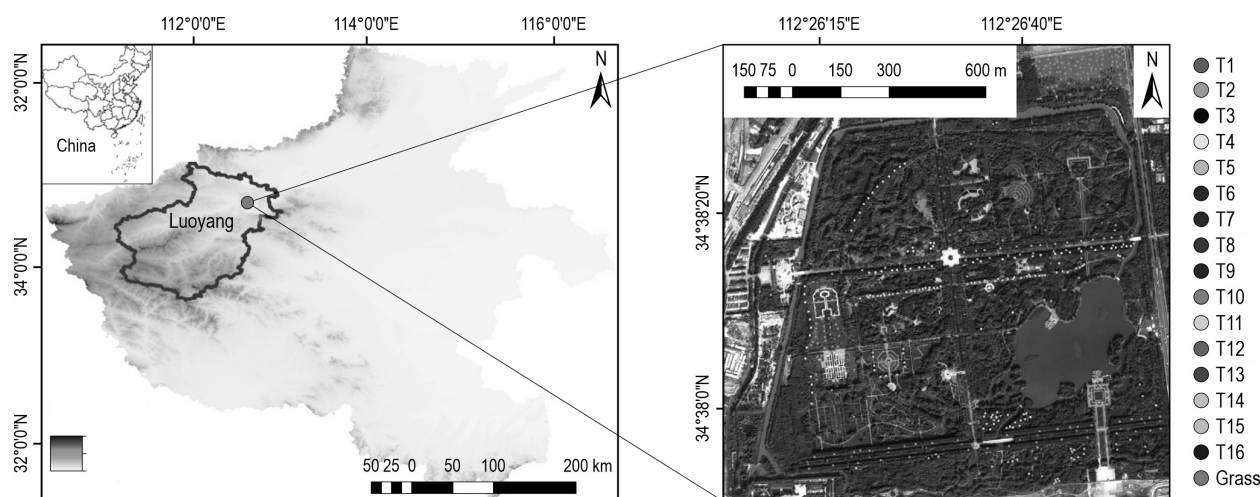


**Fig. 1** Location map of the primary study area, along with an image of the study site, illustrating the distribution of samples across various tree species. T1–T16 represent 16 tree species, and the detailed scientific names of these species are shown in Table 2

texture features. Subsequently, I combined these features with spectral bands to create various combined feature sets and high-dimensional mixed feature sets. I employed the RF classifier to assess the performance of different feature sets and rank the importance of the features within the mixed feature sets. The goal is to clarify the performance of different feature types in tree species identification and analyze the effect of their combinations on enhancing tree species identification. The research findings will provide foundational information for the adoption of robust features in tree species classification.

## 2. Materials and Methods

### 2.1 Study Area

The Botanical Garden, located within the ruins of the ancient Sui and Tang Dynasties cities in Luoyang, Henan Province, China, served as the primary exper-

imental site for my study (Fig. 1). The geographical location, temperature patterns, and annual rainfall of Luoyang, as well as the area and tree species of the study site, were thoroughly described in my previous study (Liu 2023a). An area in Hohhot City, Inner Mongolia, China, previously selected by Liu and An (2020a) for their tree species identification research, served as a test site to further validate the reliability of the Luoyang experimental results.

### 2.2 Remote Sensing Data and Pre-Processing

The primary data source for this study was a WV-3 image of Luoyang, captured on October 27, 2017. This image comprised a panchromatic band with a spatial resolution of 0.3 m and an 8-band multispectral set with a spatial resolution of 1.24 m. The detailed parameters of the WV-3 data are outlined in Table 1. As for the auxiliary data from WV-2, its band settings and wavelength ranges for each band are identical to those of the WV-3. However, the spatial resolution

**Table 1** Band configuration and spatial resolution of WV-3 imagery

Band code	Band settings	Pixel resolution size, m	Wavelength range, $\mu\text{m}$	Central wavelength
1	Coastal blue	1.24	0.40–0.45	0.425
2	Blue		0.45–0.51	0.480
3	Green		0.51–0.58	0.545
4	Yellow		0.59–0.63	0.605
5	Red		0.63–0.69	0.660
6	Red edge		0.71–0.75	0.725
7	Near-infrared 1		0.77–0.90	0.833
8	Near-infrared 2		0.86–1.04	0.950
9	Panchromatic	0.3	0.45–0.80	–

differs, with the panchromatic band at 0.5 m and the multispectral bands at 2.0 m for WV-2.

The WV-3 imagery encompassed a geographic area spanning latitudes 34°37'49.51"–34°38'35.48" N and longitudes 112°26'3.06"–112°26'58.33" E, covering a total area of 1.94 km<sup>2</sup> (Liu 2023a). Conversely, the WV-2 imagery captured a different region, spanning latitudes 40°48'11.81"–40°48'47.62" N and longitudes 111°40'55.57"–111°42'32.16" E, with a total coverage of 2.45 km<sup>2</sup> (Liu and An 2020a, Liu 2023a). Prior to utilization, both datasets underwent rigorous preprocessing steps, including calibration, image fusion, and atmospheric correction. Fig. 1 presents a visual representation of the primary study area along with its corresponding imagery.

### 2.3 Tree Species Investigation and Sample Collection

For the primary study site, a printed image was used for a field survey conducted in August 2020, revealing the potential of sixteen distinct tree species for classification (Liu 2023a). The approach for investigating tree species and labeling samples adhered to the methodology employed in our previous research in the auxiliary experimental area (Liu and An 2020a).

**Table 2** Scientific names of the tree species for classification and the number of training and validation samples used in the classification

Tree species category	Scientific names	Training samples	Validation samples
T1	<i>Sophora japonica</i>	284	5673
T2	<i>Prunus cerasifera</i> f. <i>atropurpurea</i>	280	5609
T3	<i>Salix babylonica</i>	277	5541
T4	<i>Cedrus deodara</i>	297	5939
T5	<i>Armeniaca mume</i> var. <i>mume</i> f. <i>alphandii</i>	287	5736
T6	<i>Michelia champaca</i>	291	5811
T7	<i>Sabina chinensis</i> (L.) Ant. cv. <i>Kaizuka</i>	279	5573
T8	<i>Koelreuteria paniculata</i>	293	5854
T9	<i>Eucommia ulmoides</i>	282	5648
T10	<i>Bischofia polycarpa</i>	293	5861
T11	<i>Pterocarya stenoptera</i>	292	5833
T12	<i>Platanus orientalis</i>	286	5729
T13	<i>Magnolia grandiflora</i>	285	5690
T14	<i>Metasequoia glyptostroboides</i>	285	5695
T15	<i>Fraxinus chinensis</i>	284	5685
T16	<i>Phyllostachys sulphurea</i> var. <i>Viridis</i> (bamboo)	281	5623
Grass	–	283	5656

In the main study site, the spatial distribution of these tree species and the selection of training and validation samples are detailed in the right portion of Fig. 1 and in Table 2, respectively. For the auxiliary experimental areas, details on the classified tree species and their sample collection are provided in our earlier study (Liu and An 2020a).

### 2.4 Construction of Non-Vegetation Mask

Previous research has demonstrated the ineffectiveness of the NDVI threshold method in distinguishing vegetation from blue-ground objects (Liu and An 2020b). To address this limitation, Liu and An (2020b) introduced the blue objects spectral index (BOSI) (Eq. 1), which highlights blue-ground objects in images. By setting an appropriate threshold, blue-ground objects can be accurately extracted. In the current study, I capitalized on this approach, referencing previous works (Liu and An 2020b, Liu 2023a), to construct a mask that excludes both blue-ground objects and non-vegetation areas. This mask was then applied to the images, covering non-vegetation areas, thereby minimizing their potential interference during tree species identification.

$$BOSI = (2 \times b_8 - 3 \times b_6 - b_5 - 2 \times b_4 + b_3 + 5 \times b_2 + b_1) \times [b_2 - (b_1 + b_3)/2] \quad (1)$$

Where:

$b_{1-6}$  and  $b_8$  correspond to the coastal blue, blue, green, yellow, red, red-edge, and near-infrared 2 bands of the spectral data, respectively.

### 2.5 Image Feature Set Construction

In implementing tree species classification with WV-3/2 imagery, I considered four key feature sets: (1) spectral bands (SB), (2) hue, saturation, and value (HSV) color space features (e.g., Liu and An 2019), (3) texture features (TEX) (e.g., Liu 2023a, Liu 2024), and (4) polygon area index (PAI) (Liu 2023a). The SB set was constructed from the 8-band data of the WV-3 imagery, consisting of eight spectral bands. The HSV feature set was created by randomly selecting three bands from the eight and transforming them from the RGB color space to the HSV color space. The resulting feature set contained a total of 56 HSV features (Liu and An 2019).

The TEX feature set was constructed using various texture metrics, including mean (MEA), homogeneity (HOM), variance (VAR), contrast (CON), entropy (ENT), dissimilarity (DIS), second moment (SM), and correlation (COR) (Liu et al. 2015, Liu 2022). All of these TEX features were extracted from the panchromatic

band of the WV-3 imagery, comprising a total of eight distinct features. During texture extraction, I employed the co-occurrence metrics in ENVI 5.4. The processing window dimensions were varied in accordance with a gradient ranging from  $5 \times 5$  to  $(N+2) \times (N+2)$ , where  $N$  represents the optimal window size that yields the highest overall accuracy in tree species classification over  $((N+1)/2-1)$  iterations. Specifically, I set the co-occurrence shift values for both the  $X$  and  $Y$  axes to 1. Once the eight *TEX* features were extracted from a given window, they were promptly utilized for tree species classification using MLC. The resulting overall accuracy (*OA*) was recorded to facilitate the determination of the optimal window size for texture extraction.

The construction process for the first three types of feature sets is identical for both WV-2 and WV-3 imagery. To construct the *PAI* feature set, I used Eq. (2) from Liu (2023a). Starting from band 1 of WV-3/2, I calculated the *PAIs* between band 1 and all subsequent bands (bands 2 through 8). This process was repeated for each subsequent band, calculating the *PAI* between each band and all higher-numbered bands, until the *PAI* between bands 7 and 8 was computed. This resulted in a total of 28 *PAIs* for both the WV-3 and WV-2 imagery.

$$PAI = 0.5 \times \sum_{\alpha=1}^{N-1} (b_{\alpha} + b_{\beta} - 2b_{\gamma}) \times \Delta\lambda_{\alpha\beta} \quad (2)$$

Where:

*PAI* represents the polygon area index

$N$  is the number of bands;  $\alpha = 1, 2, \dots, N-1$

$\beta = \alpha + 1$ ;  $b_{\alpha}$  represents the reflectance of the pixels in band

$\alpha$ ,  $b_{\beta}$  represents the reflectance of the pixels in band

$\alpha + 1$  by represents the band of tree species with the lowest reflectance in the  $\alpha$  to  $\beta$  band

$\Delta\lambda_{\alpha\beta}$  represents the difference between the central wavelengths of the  $\beta$  and  $\alpha$  bands.

## 2.6 Image Classification and Results Evaluation

Based on the above-constructed four types of feature sets and their combinations, the RF algorithm (Van der Linden et al. 2015) was used to identify tree species due to its excellent performance in both low-dimensional and high-dimensional feature sets for image classification. Within the mixed feature set (including 212 features), which comprises four distinct types of feature sets, all features were ranked based on their normalized importance values. These values were calculated using the variable importance measure tool provided by RF, ensuring an objective and

quantitative assessment of each feature's contribution. Optimal feature sets were identified by gradually eliminating the least important features while monitoring the classification accuracy after feature elimination, initially in groups of five, and then individually. After the classification of tree species, the validation samples served as benchmarks to evaluate the entire classification output, resulting in a confusion matrix for precision assessment. I utilized the *OA*, Kappa coefficient (*KC*), producer and user accuracy derived from this matrix, along with curve diagrams and spider graphs constructed from select metrics, to compare and analyze the nuances of the classification outcomes.

## 3. Results and Analyses

### 3.1 Optimal Window for Texture Extraction

Fig. 2 depicts the curves illustrating the relationship between the window size for texture feature extraction and the *OA* of tree species classification for the current window size.

As depicted in Fig. 2, the *OA* of tree species identification progressively increased in tandem with the expansion of the texture feature extraction window. Specifically, a window size of  $29 \times 29$  (for WV-3) and  $9 \times 9$  (for WV-2) resulted in the peak *OA* for tree species classification. However, any further increase in the window size to  $31 \times 31$  (for WV-3) and  $11 \times 11$  (for WV-2) led to a decrease in *OA*. Consequently, the texture features extracted using the optimal window size of  $29 \times 29$  (or  $9 \times 9$ ) were used in the subsequent analysis for tree species classification.

### 3.2 Tree Species Classification by Different Feature Sets

Table 3 summarizes the *OA* and *KC* of different feature types and their combinations for tree species identification.

As shown in Table 3, the texture feature set yielded the highest classification accuracy for tree species based on WV-3 single-type features, followed by the *HSV* feature set, *PAI* feature set, and spectral band set, in that order. However, for WV-2, the *HSV* feature set attained the highest recognition accuracy, surpassing the spectral bands, *PAI* feature set, and texture feature set, in that order. Notably, the effectiveness of these feature sets in classifying tree species across different images remains unclear based solely on these results.

In the identification of tree species using combinations of two feature sets, the texture feature set combined with spectral bands, *PAI*, and *HSV* sets achieved

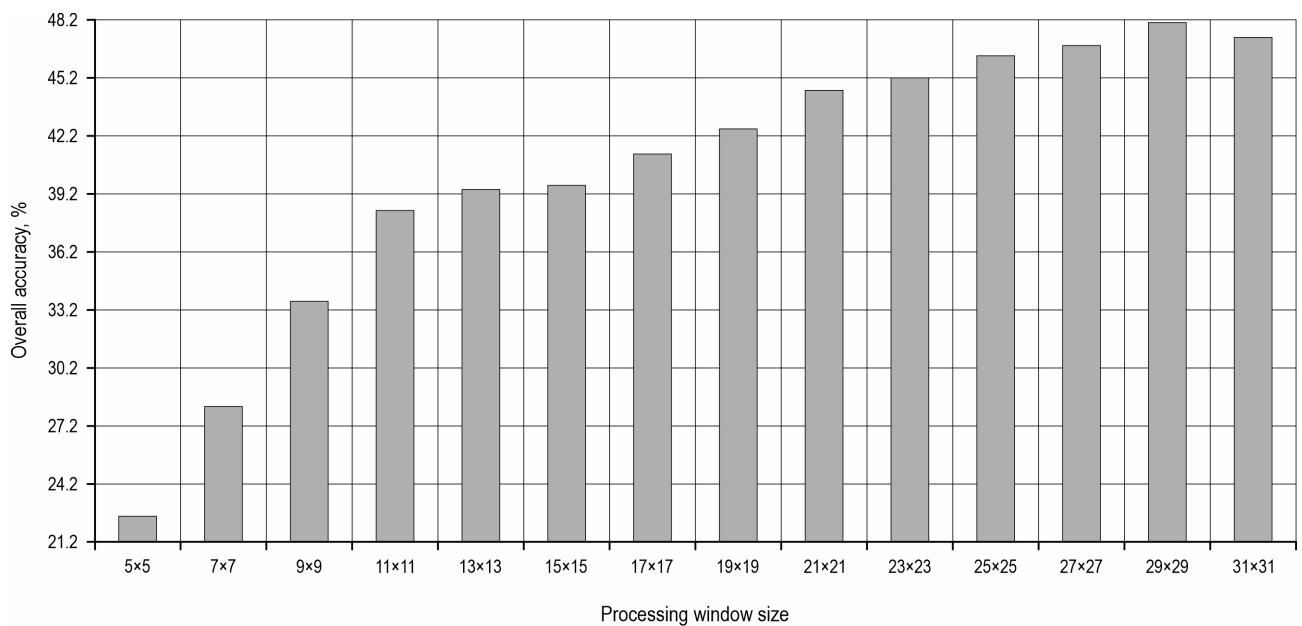


**Fig. 2** Determination of the optimal window size for texture feature extraction. Change in *OA* with varying window sizes for eight types of texture extraction in WV-3 panchromatic band. The *OA* of tree species classification initially increases with window size, peaking at 29×29 before declining, indicating the existence of an optimal scale for capturing textural information

**Table 3** Overall accuracy and *KC* achieved in tree species classification based on various feature sets

Feature sets	WV-3		WV-2	
	<i>OA</i> , %	<i>KC</i>	<i>OA</i> %	<i>KC</i>
8 <i>SBs</i>	65.87	0.6374	76.78	0.7289
28 <i>PAIs</i>	70.61	0.6877	76.44	0.7248
56 <i>HSV</i> s	75.76	0.7424	78.27	0.7463
8 <i>TEX</i> s	76.64	0.7518	70.91	0.6598
8 <i>SBs</i> +28 <i>PAIs</i>	73.53	0.7188	78.74	0.7517
8 <i>SBs</i> +56 <i>HSV</i> s	75.74	0.7422	78.08	0.7441
8 <i>SBs</i> +8 <i>TEX</i> s	86.10	0.8523	82.70	0.7978
28 <i>PAIs</i> +56 <i>HSV</i> s	76.24	0.7475	78.21	0.7456
28 <i>PAIs</i> +8 <i>TEX</i> s	89.49	0.8883	83.33	0.8052
56 <i>HSV</i> s+8 <i>TEX</i> s	87.86	0.8710	82.73	0.7982
8 <i>SBs</i> +28 <i>PAIs</i> +56 <i>HSV</i> s	76.19	0.7470	78.43	0.7482
8 <i>SBs</i> +28 <i>PAIs</i> +8 <i>TEX</i> s	89.40	0.8874	83.80	0.8107
8 <i>SBs</i> +56 <i>HSV</i> s+8 <i>TEX</i> s	88.02	0.8727	82.89	0.8000
28 <i>PAIs</i> +56 <i>HSV</i> s+8 <i>TEX</i> s	87.87	0.8711	83.06	0.8021
8 <i>SBs</i> +28 <i>PAIs</i> +56 <i>HSV</i> s+8 <i>TEX</i> s	88.12	0.8738	82.73	0.7982

high accuracy, ranging from 86.10% to 89.49% for WV-3 and 82.70% to 83.33% for WV-2. Specifically, the combination of the texture and *PAI* feature sets yielded the highest accuracy, achieving 89.49% for WV-3 and 83.33% for WV-2. Conversely, the combinations of

spectral bands with *PAIs*, *HSV*s, and *PAI* combined with *HSV* feature sets did not significantly enhance the classification accuracy.

In tree species identification, the combination of three types of feature sets did not yield any further

improvement in accuracy compared to the combinations of two or fewer feature sets. Moreover, when combining all four types of feature sets for tree species classification, the *OA* declined slightly to 88.12% for WV-3 and 82.73% for WV-2, compared to the optimal results achieved with fewer feature sets (89.49% for WV-3 and 83.80% for WV-2).

### 3.3 Key Features for Tree Species Identification

Utilizing the RF algorithm, I ranked the importance of all features in the mixed feature set for WV-3, highlighting the top 100 in Table 4. Then, I conducted tree species classification using these top 100 features, elim-

inating sets of 5 features in descending order of importance. Fig. 3(a) depicts the changes in *OA* as features are sequentially removed in increments of 5, while Fig. 3(b) zooms in on the *OA* variation for each individual feature that is eliminated, based on the optimal interval determined at every 5-feature elimination step.

As shown in Fig. 3(a), as lower-ranked features were eliminated, the *OA* for tree species classification generally increased, peaking at the top 35 features. Subsequent removal of more important features led to a decline in the *OA*, suggesting that the optimal feature set for tree species identification consists of approximately 35 of the top 100 features.

**Table 4** The top 100 most important features for WV-3 tree species classification as ranked by the random forest classifier. The dominance of texture features (e.g., VAR, MEA, DIS) in the highest ranks and the significant presence of *HSV* features (prefix 'H', 'S', 'V') underscore their critical role, while the absence of spectral bands (*SB*) until rank 100 highlights their relative inferiority

Feature	Importance value	Ranking	Feature	Importance value	Ranking	Feature	Importance value	Importance ranking	Feature	Importance value	Ranking
VAR	1.66	1	V 237	0.78	26	PAI 4 to 5	0.66	51	H 246	0.56	76
MEA	1.52	2	PAI 6 to 7	0.77	27	S 123	0.66	52	H 235	0.56	77
DIS	1.51	3	H 578	0.77	28	H 367	0.65	53	H 127	0.56	78
HOM	1.49	4	H 368	0.77	29	H 148	0.65	54	S 568	0.55	79
CON	1.48	5	H 257	0.77	30	H 457	0.64	55	S 346	0.54	80
ENT	1.38	6	S 245	0.77	31	H 567	0.63	56	S 136	0.54	81
SM	1.38	7	H 356	0.76	32	S 235	0.63	57	H 135	0.54	82
COR	1.19	8	PAI 6 to 8	0.75	33	H 157	0.63	58	S 368	0.53	83
H 678	0.95	9	PAI 2 to 5	0.74	34	H 126	0.63	59	V 348	0.53	84
H 478	0.95	10	H 237	0.73	35	S 345	0.62	60	H 147	0.53	85
PAI 1 to 5	0.87	11	H 238	0.72	36	H 167	0.62	61	PAI 4 to 8	0.52	86
H 378	0.87	12	PAI 3 to 5	0.70	37	H 467	0.61	62	S 146	0.52	87
H 267	0.87	13	PAI 2 to 4	0.70	38	S 456	0.61	63	PAI 2 to 7	0.51	88
H 258	0.87	14	H 456	0.70	39	H 247	0.61	64	S 467	0.51	89
H 357	0.86	15	H 256	0.70	40	S 234	0.61	65	PAI 2 to 6	0.50	90
H 348	0.86	16	S 145	0.70	41	S 124	0.61	66	S 478	0.50	91
H 268	0.86	17	S 135	0.70	42	H 146	0.6	67	S 358	0.50	92
PAI 7 to 8	0.84	18	H 156	0.69	43	H 568	0.59	68	S 356	0.50	93
H 358	0.84	19	H 136	0.69	44	H 458	0.58	69	S 267	0.50	94
H 178	0.84	20	PAI 2 to 3	0.68	45	S 458	0.58	70	S 257	0.50	95
H 168	0.84	21	PAI 1 to 6	0.68	46	H 128	0.58	71	S 178	0.50	96
S 125	0.80	22	PAI 1 to 3	0.68	47	S 367	0.57	72	S 156	0.50	97
S 678	0.78	23	H 236	0.68	48	S 457	0.56	73	S 137	0.50	98
H 468	0.78	24	S 134	0.68	49	S 378	0.56	74	S 128	0.50	99
H 278	0.78	25	H 347	0.67	50	H 346	0.56	75	SB 5	0.49	100

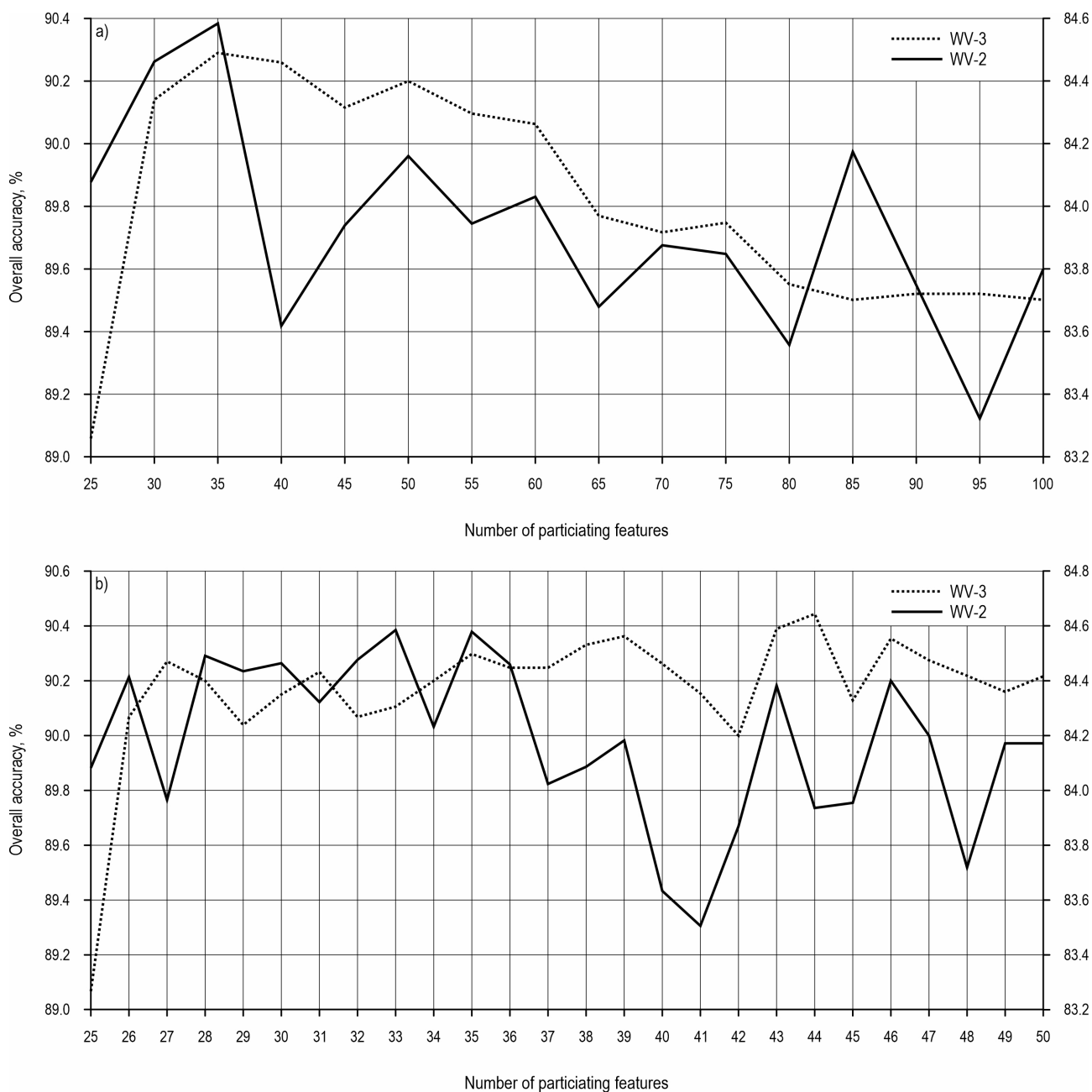


**Fig. 3** Identification of the optimal feature set through backward feature elimination. (a) The OA achieved in tree species identification by the latest feature set after removing every five lowest-ranked features (from ranks 25 to 100). The OA peaks when the top ~35 most important features are used, demonstrating that a compact, discriminative feature subset exists; (b) the OA achieved in tree species identification by the latest feature set after removing every one of the lowest-ranked features (from ranks 25 to 50). Fine-tuning reveals the exact optimal number of features (44 for WV-3, 33 for WV-2), beyond which the removal of any more important features causes a performance drop. The left and right vertical axes in the figure represent the classification accuracy for WV-3 and WV-2, respectively

Beginning with the 35<sup>th</sup> most important feature, I expanded the potential optimal feature set by including the top 50 features in descending order of importance. Among these top 50 features, I eliminated the less important ones one by one. Experimental results

revealed that using the top 44 features (33 for WV-2) for tree species classification yielded the highest OA, thus constituting the optimal feature set.

Based on Table 4 and the experimental results for WV-2, among the optimal feature sets for tree species

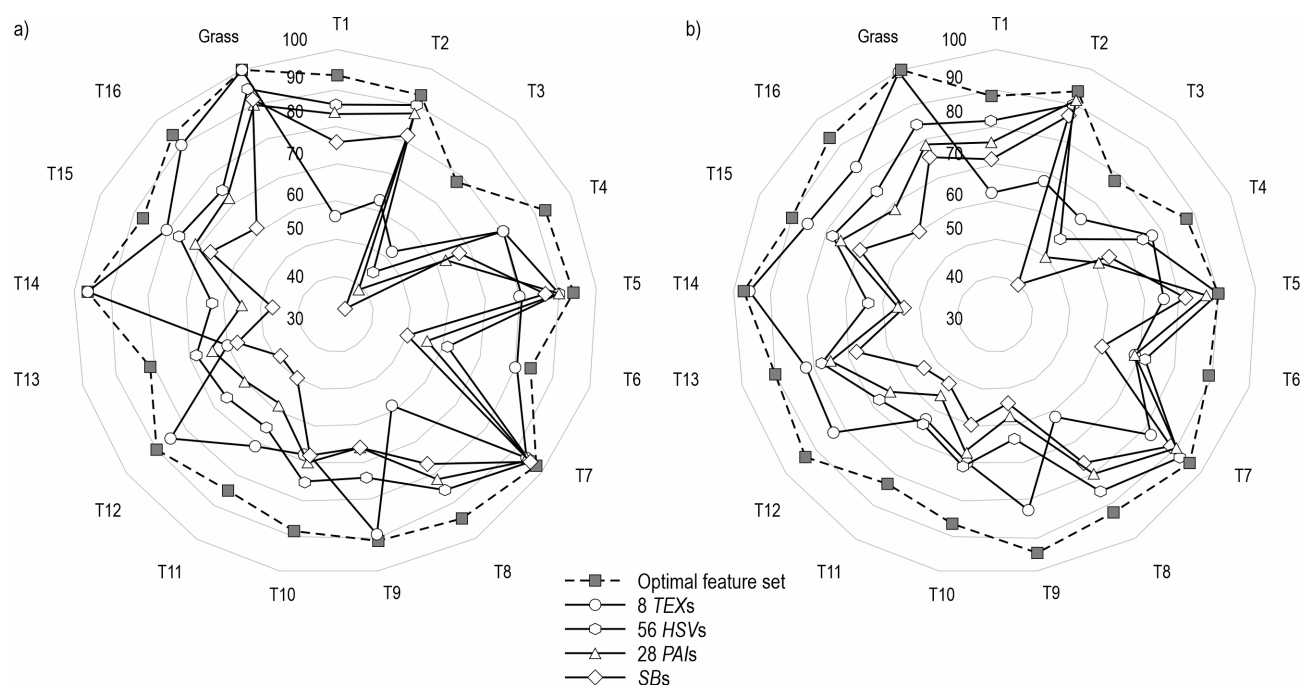


**Fig. 4** Comparative performance of different feature sets for individual species: Spider web graphs of (a) producer accuracy and (b) user accuracy show that the optimal feature set (dash line) consistently achieves high and balanced accuracy across most tree species, whereas single-type feature sets (e.g., *TEXs*, *HSV*s) exhibit high variability and species-specific strengths and weaknesses

classification (top 44 for WV-3, 33 for WV-2), all eight texture features were selected, primarily at the forefront, accounting for 18.20% (24.24% for WV-2). Additionally, 7 (4 for WV-2) *PAI* features were selected, representing 15.91% (12.12% for WV-2) of the total. Most prominently, 29 (21 for WV-2) *HSV* features were selected, comprising 65.91% (63.64% for WV-2) of the optimal set. Notably, no spectral bands were selected in either case.

### 3.4 Tree Species Identification Comparison of Typical Data Sets

Taking WV-3 as an example, Fig. 4 (a) and (b) display the producer and user accuracy spider web graphs, respectively, generated using the optimal feature set, 8 *TEX*s, 56 *HSV*s, 28 *PAI*s, and 8 spectral bands. Fig. 5 depicts the tree species identification results achieved with these representative feature sets.

As depicted in Fig. 4, for the recognition of T14, the producer accuracy of the optimal feature set was slightly lower than that achieved using only 8 *TEX* features. Similarly, for grass recognition, the user accuracy was also slightly lower compared to using 8 *TEX* features. However, when identifying any tree species or grass, the producer and user accuracy of the optimal feature set outperformed those of the other four single-type feature sets. Among the various fea-

ture sets, different combinations exhibited varying recognition effects for the same tree species, resulting in significant differences in both producer and user accuracy for tree species identification.

By combining the information from Figs. 4 and 5, it is evident that in the identification of tree species using single-class feature sets, the recognition performance of 8 *TEX* features for tree species T1, T2, T5, and T8 was significantly inferior compared to that of other feature sets. However, for tree species T6, T9, T11, T12, T14, and T16, the recognition performance of 8 *TEX* features was notably superior to that of the other feature sets. The 56 *HSV* features demonstrated better recognition effects for most tree species compared to 28 *PAI* features and eight spectral bands. Specifically, 28 *PAI* features excelled in the recognition of T5 and T7, outperforming the other feature sets. The optimal feature set, by effectively integrating the strengths of each feature group, achieved excellent recognition results across all tree species and grasses.

### 3.5 The Optimal Classification Result Analysis

Utilizing the optimal WV-3 feature set, comprising 44 features, for the classification of tree species and grass, the resulting confusion matrix is presented in Table 5, and the corresponding classification map is depicted in Fig. 5(b).

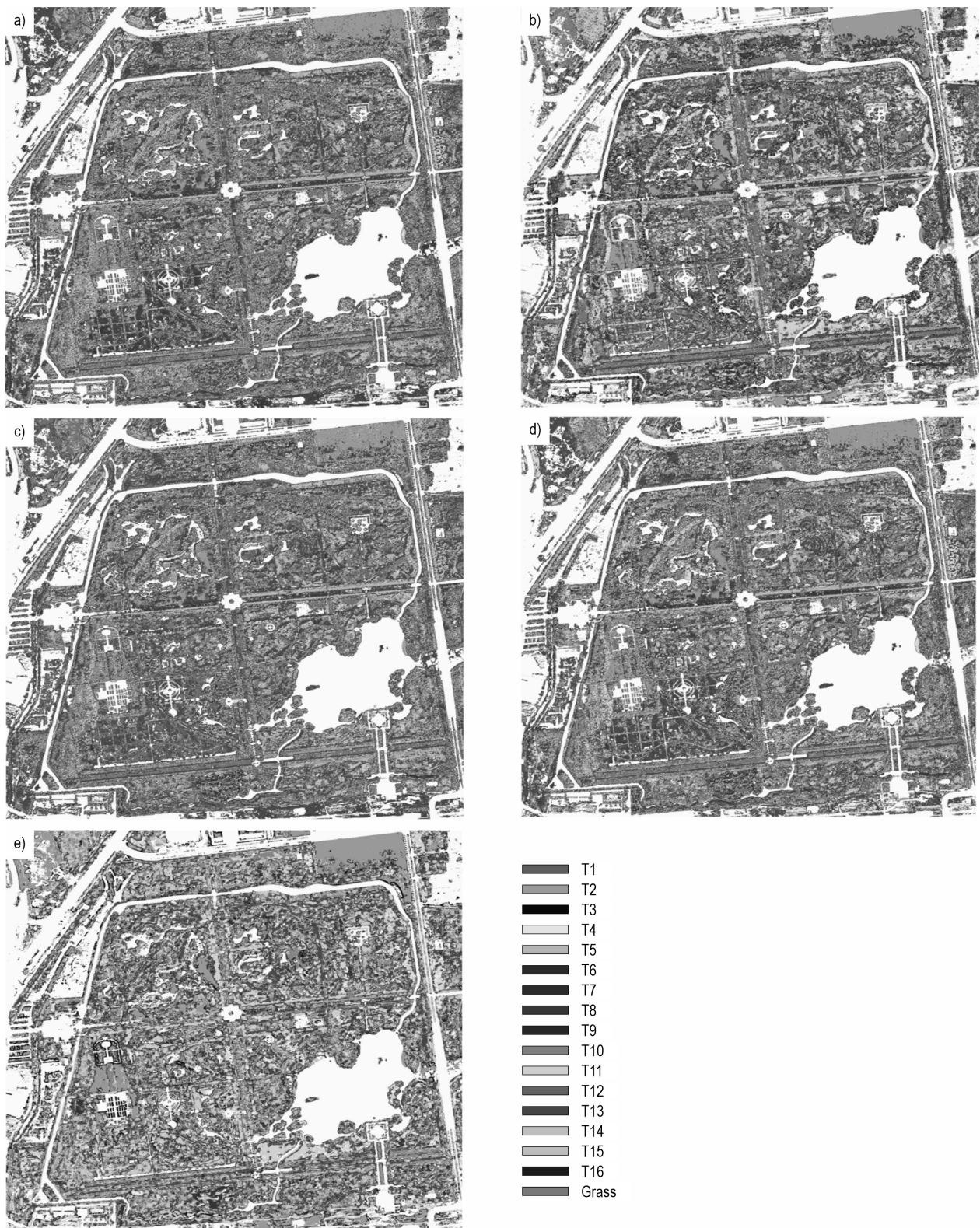


**Fig. 5** Visual comparison of classification results using different feature sets. (a) Spectral bands alone result in a noisy and speckled output. (b) The optimal feature set produces a spatially coherent and homogeneous map, closely resembling the expected distribution of tree stands. (c–e) Classification maps from single-type features (28 PAIs, 56 HSVs, and 8 TEXs, respectively) show intermediate levels of noise and misclassification, highlighting the superiority of the multi-feature approach

**Table 5** Confusion matrix for classification using the optimal feature set (44 features) with WV-3 imagery. The model achieves an excellent OA of 90.45%, with most tree species attaining both producer and user accuracy above 85%

Type	T1	T2	T3	T4	T5	T6	T7	T8	T9	T10	T11	T12	T13	T14	T15	T16	Grass
T1	5304	0	130	21	0	30	2	0	3	0	34	60	45	6	334	30	0
T2	0	5193	0	5	307	0	11	15	0	0	1	0	2	0	0	0	0
T3	61	0	4316	136	0	228	6	60	9	80	127	43	307	20	93	41	1
T4	21	0	235	5483	0	59	76	0	77	0	53	30	74	96	21	27	0
T5	0	387	0	1	5357	11	23	58	0	0	2	2	0	0	0	0	0
T6	31	0	156	3	0	4876	1	15	0	0	1	191	61	32	77	1	0
T7	28	0	86	66	1	1	5383	7	40	0	0	0	11	0	0	0	0
T8	1	14	20	0	70	164	39	5485	1	19	46	39	55	1	1	0	27
T9	13	14	19	54	1	0	23	0	5158	68	43	29	16	0	0	16	0
T10	0	1	119	0	0	3	0	165	31	5215	316	2	130	0	7	49	0
T11	5	0	157	62	0	36	0	39	251	295	4960	9	108	0	30	43	0
T12	68	0	35	1	0	160	0	0	6	0	10	5151	2	23	136	4	0
T13	5	0	63	47	0	44	9	3	35	162	139	0	4626	12	4	73	0
T14	0	0	4	50	0	75	0	0	0	0	0	22	74	5466	6	19	0
T15	136	0	145	5	0	109	0	2	0	0	3	151	55	39	4965	6	2
T16	0	0	56	5	0	15	0	0	37	22	98	0	124	0	11	5314	0
Grass	0	0	0	0	0	0	0	5	0	0	0	0	0	0	0	0	5626
Row total	5999	5534	5528	6252	5841	5445	5623	5982	5454	6038	5995	5596	5222	5716	5618	5682	5631
Column total	5673	5609	5541	5939	5736	5811	5573	5854	5648	5861	5833	5729	5690	5695	5685	5623	5656
User accuracy, %	88.41	93.84	78.08	87.70	91.71	89.55	95.73	91.69	94.57	86.37	82.74	92.05	88.59	95.63	88.38	93.52	99.91
Producer accuracy, %	93.50	92.58	77.89	92.32	93.39	83.91	96.59	93.70	91.32	88.98	85.03	89.91	81.30	95.98	87.34	94.50	99.47

OA =  $87,878/97,156 = 90.45\%$ ; KC = 0.8985.

From Table 5, it is evident that the producer accuracy for the classification of 16 tree species/bamboo and grass using the optimal feature set ranged from 77.89% (T3) to 99.47% (grass). Notably, 14 of these tree species/grass achieved producer accuracy exceeding 85%. Similarly, the user accuracy ranged from 78.08% (T3) to 99.91% (grass), with 15 tree species/bamboo and grass having user accuracy surpassing 85%. Specifically, the producer accuracy and user accuracy for tree species T3 were closely aligned, yet significantly lower than those of the other tree species/grass. For the remaining species, the difference between producer and user accuracy was relatively minor.

#### 4. Discussion

The accuracy of tree species classification was constrained when relying solely on WV-3/2 single-type features (Table 3). Nevertheless, the discovery of new features, such as PAI, and the integration of multiple feature types, offer promising avenues for improving tree species identification (Table 5). Experimental

results reveal that texture, HSV, and PAI features constitute a significant portion of the top 100 and optimal feature sets, with relatively high rankings. This underscores their positive contribution to tree species classification and identifies them as the primary drivers of accurate recognition (Table 4). Conversely, the highest-ranked spectral band only attained the 100<sup>th</sup> position in the mixed feature set, and no spectral bands were included in the optimal set. This suggests that spectral bands played a less crucial role compared to the other three feature types in tree species classification.

Using the optimal feature set for tree species recognition, texture features emerged as a crucial factor, with eight types of textures ranking highly. This underscores the significant role texture plays in tree species classification, aligning with findings from numerous contemporary studies (e.g., Pu and Landry 2012, Liu et al. 2015). Notably, this research further validates the vital importance of HSV in tree species classification. Prior to this, our previous work using WV-2 data had already established HSV's positive contribution (Liu and An 2019), but this is the first comprehensive evidence, beyond our own studies,

demonstrating *HSV*'s significant role. In the optimal feature set, *HSV* features comprised a total of 29 instances (21 for WV-2), with Hue, Sat, and Val accounting for 23 (18), 5 (3), and 1 (0), respectively. The preponderance of Hue features suggests that they have the greatest impact on tree species identification, likely due to the distinctive leaf tones among various species. Furthermore, the varying degrees of color saturation exhibited by different tree leaves provide a compelling explanation for how Sat features contribute to tree species recognition.

A detailed examination of the confusion matrix (Table 5) reveals significant variations in classification accuracy among the sixteen tree species. This disparity can be attributed to a combination of ecological traits and their manifestations in remote sensing data. Species with distinct structural characteristics, such as T7 and T14, which have unique, easily identifiable crown shapes and textures (columnar and conical, respectively), were classified with high accuracy (Producer accuracy: 96.59% and 95.98%). Their distinct textural signatures, effectively captured by the *TEX* features, made them spectrally and spatially separable from others. Conversely, species that were prone to misclassification, such as T3, likely share similar spectral and structural properties with other species. For instance, T3 was most frequently confused with T13 and T1. This confusion may stem from overlapping canopy structures and leaf morphologies that result in analogous texture responses, as well as potentially similar leaf biochemical properties leading to convergent spectral signatures in the WV-3 bands. The fact that these species were all classified within the same botanical garden under identical environmental conditions further suggests that their intrinsic spectral-structural similarity is the primary challenge. Furthermore, the exceptional accuracy in distinguishing grass from all tree species ( $PA > 99.5\%$ ) underscores the model's proficiency in separating vegetation classes with fundamentally different life forms and canopy characteristics. This analysis indicates that future classification strategies can be improved by pre-identifying and focusing on such »confusion species groups«. For these groups, incorporating more targeted features, such as those derived from phenological changes (using multi-temporal imagery) or from higher-fidelity spectral data, may be necessary to resolve the ambiguity.

This research further validates the positive role played by the newly developed *PAI* in the identification of tree species (Tables 3 and 4). While previous studies (Liu 2023a) have assessed the significance of *PAIs* in tree species classification, the scope of the compared features was relatively narrow, focusing primarily on spectral bands and texture. Notably, the perfor-

mance of texture features was hindered due to their extraction using a 3×3 window and the utilization of only a single type of texture feature, »mean«. In contrast, the current study comprehensively evaluates four diverse feature types: *PAI*, spectral bands, texture, and *HSV*, all of which are widely utilized in tree species identification (Wang et al. 2016, Liu and An 2019). Furthermore, eight distinct types of texture features were extracted using an optimized window size. Despite the inclusion of these additional important features, *PAIs* remain a crucial component of the optimal feature set, reaffirming their capability to enhance the accuracy of tree species identification. The fact that 7 (4 for WV-2) *PAI* features were selected for the optimal 44-feature (33-feature for WV-2) set (Table 4), accounting for 15.91% (12.12% for WV-2) of its composition, is particularly noteworthy. This demonstrates that *PAI* provides unique and complementary information not fully captured by other, more established features. The behavior of the *PAI* can be elucidated by considering its formulation. Unlike spectral bands, which measure reflectance at discrete wavelengths, or *HSV*, which transforms color space, the *PAI* captures the shape of the spectral curve between two bands. For instance, *PAI* 1 to 5 (ranking 11<sup>th</sup> in importance) calculates the area between the Coastal Blue and Red bands. A large area in this region of the spectrum might indicate a species with a steeper slope in the blue-to-green transition, a characteristic that could be linked to specific leaf pigments or structures. This allows *PAI* to differentiate species that might have similar reflectance in a few bands but different overall spectral shapes. A specific example from my results supports this: the strong performance of *PAI* features likely contributed to the accurate discrimination of T5 and T7, species for which the 28 *PAIs* alone showed notable proficiency (Fig. 4), suggesting that their spectral curves have distinctive polygon areas that set them apart from other species. Its integration with texture features, in particular, yielded one of the highest accuracies among two-feature set combinations (89.49% for WV-3, 83.33% for WV-2, Table 3). This synergy suggests that *PAI* (capturing spectral curve morphology) and texture (capturing spatial patterns) describe orthogonal and complementary aspects of tree species characteristics, making their combination exceptionally powerful.

In this study, a mixed feature set comprising four types of textures totaled 212 features. When using this mixed feature set for tree species classification, the *OA* was only 88.12% (82.73% for WV-2) (Table 3). However, after undergoing a rigorous feature selection process, an optimal feature set was identified, containing only 44 features (33 for WV-2) (Fig. 3). Remarkably, when using this reduced but effective set of fea-

tures, the accuracy of tree species classification increased to 90.45% (84.60% for WV-2) (Table 5), indicating the significant impact of feature selection. By employing fewer but targeted features, not only did I achieve higher classification accuracy, but I also reduced the computational burden, a crucial consideration when dealing with high-dimensional datasets for tree species classification.

While this study demonstrates the effectiveness of the multi-feature combination and the utility of *PAI* and *HSV* features in tree species classification using WorldView-2/3 imagery, it is important to acknowledge its limitations regarding the sensors, as well as the spatial and temporal representativeness of the datasets. Regarding the sensors, my methodology and conclusions are based primarily on WorldView-2/3 imagery. The high spatial and spectral resolution of these sensors is crucial for extracting the texture and *PAI* features that proved to be highly important. The performance might vary if applied to data from other satellites (e.g., Sentinel-2 or Landsat-8/9) with different band settings, spatial resolutions, and radiometric characteristics, which could affect the importance of *HSV* and *PAI* features, as well as textures. Regarding the spatial and temporal representativeness, my validation was conducted in two specific geographical locations (Luoyang and Hohhot) during a particular season (primarily autumn for the main site). The effectiveness of the features, especially those related to color (*HSV*) and phenology (which influences spectral curves and thus *PAI*), might vary across different climatic zones, forest ecosystems, and seasons. Therefore, the distinct hues that proved to be highly important in my study might be less discernible among tree species in a tropical rainforest or during the lush summer canopy. Therefore, the current conclusions about feature importance are most directly applicable to temperate urban botanical gardens with similar species composition and imaging conditions. The robustness of the proposed optimal feature set under different sensor configurations, environmental conditions, and across multiple growing seasons remains to be verified. Given the limitations of the current study, future work will focus on evaluating the approach with a wider range of datasets from various seasons and regions to further assess the contribution of features, particularly *HSV* and *PAI*, to tree species classification.

## 5. Conclusions

The effectiveness of the newly developed *PAIs*, when combined with spectral bands, *HSVs*, and texture features was tested for tree species identification. This study also determined the importance of different

features in tree species identification. To achieve the results, WV-3/2 data were used to construct spectral band sets, *PAI* sets, *HSV* sets and texture feature sets, along with several mixed feature sets derived from them. Subsequently, the RF classifier was used to classify tree species based on the various feature sets and assess the importance of these features involved in the classifications. The experimental results led to the following conclusions:

- ⇒ compared to single-type features, the combination of multiple feature types from remote sensing data outperforms them in effectively identifying tree species
- ⇒ texture features play a crucial role in tree species identification, and numerous *HSV* features were also significantly important. However, the positive impact of spectral band features, by contrast, was not as pronounced
- ⇒ notably, many *PAI* features were part of the optimal feature sets for tree species recognition, indicating that the newly developed *PAI* features were also highly significant in tree species classification.

The experimental results indicate that combining multiple features of remote sensing data for tree species classification improves identification accuracy. Specifically, *HSV* features and the newly proposed *PAI* features should be given high consideration in subsequent studies for tree species classification. Furthermore, additional research is needed to determine which bands of remote sensing data yield the most beneficial *HSV* and *PAI* features for tree species classification, enabling their direct application in practical settings and future research. Moreover, to fully establish the robustness and generalizability of these findings, future studies should validate the proposed feature selection and classification framework across diverse sensors, geographic regions, forest types, and seasonal conditions.

## Acknowledgements

Funding: This work was supported by the Scientific and Technological Project of Henan Province, China (Grant Nos. 262102320247, 242102320027), and the National Natural Science Foundation of China (Grant No. 32001250). I want to express my gratitude to the editors and the anonymous reviewers.

## 6. References

Åkerblom, M., Raunonen, P., Mäkipää, R., Kaasalainen, M., 2017: Automatic tree species recognition with quantitative structure models. *Eur. J. For. Res.* 191: 1–12. <https://doi.org/10.1016/j.rse.2016.12.002>

- Apostol, B., Petrila, M., Lorent, A., Ciceu, A., Gancz, V., Badea, O., 2020: Species discrimination and individual tree detection for predicting main dendrometric characteristics in mixed temperate forests by use of airborne laser scanning and ultra-high-resolution imagery. *Sci. Total Environ.* 698: 134074. <https://doi.org/10.1016/j.scitotenv.2019.134074>
- Carvalho, M.D., Marcato, J., Martins, J.A.C., Zamboni, P., Costa, C.S., Siqueira, H.L., Araújo, M.S., Gonçalves, D.N., Furuya, D.E.G., Osco, L.P., Ramos, A.P.M., Li, J., Castro, A.A.D., Gonçalves, W.N., 2022: A deep learning-based mobile application for tree species mapping in RGB images. *Int. J. Appl. Earth Obs. Geoinf.* 114: 103045. <https://doi.org/10.1016/j.jag.2022.103045>
- Cross, M.D., Scambos, T., Pacifici, F., Marshall, W.E., 2019: Determining effective meter-scale image data and spectral vegetation indices for tropical forest tree species differentiation. *IEEE J. Sel. Top. Appl. Earth Obs. Remote Sens.* 12(8): 2934–2943. <https://doi.org/10.1109/JSTARS.2019.2918487>
- Ferreira, M.P., Wagner, F.H., Aragão, L.E.O.C., Shimabukuro, Y.E., Filho, C.R.D.S., 2019: Tree species classification in tropical forests using visible to shortwave infrared WorldView-3 images and texture analysis. *ISPRS J. Photogramm. Remote Sens.* 149: 119–131. <https://doi.org/10.1016/j.isprsjprs.2019.01.019>
- Ghosh, A., Joshi, P.K., 2014: A comparison of selected classification algorithms for mapping bamboo patches in lower Gangetic plains using very high resolution WorldView-2 imagery. *Int. J. Appl. Earth Obs. Geoinf.* 26(1): 298–311. <https://doi.org/10.1016/j.jag.2013.08.011>
- Hamraz, H., Jacobs, N.B., Contreras, M.A., Clark, C., 2019: Deep learning for conifer/deciduous classification of airborne LiDAR 3D point clouds representing individual trees. *ISPRS J. Photogramm. Remote Sens.* 158: 219–230. <https://doi.org/10.1016/j.isprsjprs.2019.10.011>
- Han, W., Zhang, S., Jiao, Q., Wu, H., 2019: Dominant tree species mapping based on multi-temporal CHRIS hyperspectral satellite data. *Forest Inventory and Planning* 44(2): 1–6.
- Immitzer, M., Neuwirth, M., Böck, S., Brenner, H., Vuolo, F., Atzberger, C., 2019: Optimal input features for tree species classification in central Europe based on multi-temporal sentinel-2 data. *Remote Sens.* 11(22): 2599. <https://doi.org/10.3390/rs11222599>
- Kemal, A., Serhat, K., Onur, C., 2019: Classification and diagnosis of cervical cancer with stacked autoencoder and softmax classification. *Expert Syst. Appl.* 115: 557–564. <https://doi.org/10.1016/j.eswa.2018.08.050>
- Kureel, N., Sarup, J., Matin, S., Goswami, S., Kureel, K., 2022: Modelling vegetation health and stress using hyperspectral remote sensing data. *Model. Earth Syst. Environ.* 8(1): 733–748. <https://doi.org/10.1007/s40808-021-01113-8>
- Kwon, R., Ryu, Y., Yang, T., Zhong, Z.L., Im, J., 2023: Merging multiple sensing platforms and deep learning empowers individual tree mapping and species detection at the city scale. *ISPRS J. Photogramm. Remote Sens.* 206: 201–221. <https://doi.org/10.1016/j.isprsjprs.2023.11.011>
- Liu, H., 2022: Classification of urban tree species using multi-features derived from four-season RedEdge-MX data. *Comput. Electron. Agric.* 194: 106794. <https://doi.org/10.1016/j.compag.2022.106794>
- Liu, H., 2023a: Effectiveness of the spectral area index created by three algorithms for tree species recognition. *Ann. For. Sci.* 80(1): 17. <https://doi.org/10.1186/s13595-023-01184-w>
- Liu, H., 2023b: Spectral volume index creation and performance evaluation: a preliminary test for tree species identification. *Heliyon* 9(6): e17203. <https://doi.org/10.1016/j.heliyon.2023.e17203>
- Liu, H., 2024: Classification of tree species using UAV-based multi-spectral and multi-seasonal images: a multi-feature-based approach. *New For.* 55(1): 173–196. <https://doi.org/10.1007/s11056-023-09974-w>
- Liu, H., An, H., 2019: Urban greening tree species classification based on HSV colour space of WorldView-2. *J. Indian Soc. Remote Sens.* 47(11): 1959–1967. <https://doi.org/10.1007/s12524-019-01028-z>
- Liu, H., An, H., 2020a: Analysis of the importance of five new spectral indices from WorldView-2 in tree species classification. *J. Spatial Sci.* 65(3): 455–466. <https://doi.org/10.1080/14498596.2018.1521754>
- Liu, H., An, H., 2020b: Extraction of four types of urban ground objects based on a newly created WorldView-2 multi-colour spectral index. *J. Indian Soc. Remote Sens.* 48(7): 1091–1100. <https://doi.org/10.1007/s12524-020-01134-3>
- Liu, H.P., An, H.J., Wang, B., Zhang, Q.L., 2015: Tree species classification using WorldView-2 images based on recursive texture feature elimination. *J. Beijing For. Univ.* 37(8): 53–59. <https://doi.org/10.13332/j.1000-1522.20140311>
- Masemola, C., Cho, M.A., Ramoelo, A., 2019: Assessing the effect of seasonality on leaf and canopy spectra for the discrimination of an alien tree species, *acacia mearnsii*, from co-occurring native species using parametric and nonparametric classifiers. *IEEE Trans. Geosci. Remote Sens.* 57(8): 5853–5867. <https://doi.org/10.1109/TGRS.2019.2902774>
- Modzelewska, A., Fassnacht, F.E., Stereńczak, K., 2020: Tree species identification within an extensive forest area with diverse management regimes using airborne hyperspectral data. *Int. J. Appl. Earth Obs. Geoinf.* 84: 101960. <https://doi.org/10.1016/j.jag.2019.101960>
- Naidoo, L., Cho, M.A., Mathieu, R., Asner, G.P., 2012: Classification of savanna tree species, in the Greater Kruger National Park region, by integrating hyperspectral and LiDAR data in a Random Forest data mining environment. *ISPRS J. Photogramm. Remote Sens.* 69(3): 167–179. <https://doi.org/10.1016/j.isprsjprs.2012.03.005>
- Pu, R., Landry, S., 2012: A comparative analysis of high resolution IKONOS and WorldView-2 imagery for mapping

urban tree species. *Remote Sens. Environ.* 124: 516–533. <https://doi.org/10.1016/j.rse.2012.06.011>

Pu, R., Shawn, L., Yu, Q., 2018: Assessing the potential of multi-seasonal high resolution pléiades satellite imagery for mapping urban tree species. *Int. J. Appl. Earth Obs. Geoinf.* 71: 144–158. <https://doi.org/10.1016/j.jag.2018.05.005>

Richards, J.A., Jia, X., 2008: Using suitable neighbors to augment the training set in hyperspectral maximum likelihood classification. *IEEE Geosci. Remote Sens. Lett.* 5(4): 774–777. <https://doi.org/10.1109/LGRS.2008.2005512>

Shi, Y.F., Wang, T.J., Skidmore, A.K., Heurich, M., 2020: Improving LiDAR-based tree species mapping in Central European mixed forests using multi-temporal digital aerial colour-infrared photographs. *Int. J. Appl. Earth Obs. Geoinf.* 84: 101970. <https://doi.org/10.1016/j.jag.2019.101970>

Torabzadeh, H., Leiterer, R., Hueni, A., Schaepman, M., Morsdorf, F., 2019: Tree species classification in a temperate mixed forest using a combination of imaging spectroscopy and airborne laser scanning. *Agric. For. Meteorol.* 279: 107744. <https://doi.org/10.1016/J.AGRFORMET.2019.107744>

Van der Linden, S., Rabe, A., Held, M., Jakimow, B., Leitão, P.J., Okujeni, A., Schwieder, M., Suess, S., Hostert, P., 2015:

The EnMAP-box- A toolbox and application programming interface for EnMAP data processing. *Remote Sens.* 7(9): 11249–11266. <https://doi.org/10.3390/rs70911249>

Wang, T., Zhang, H., Lin, H., Fang, C., 2016: Textural-spectral feature-based species classification of mangroves in mai po nature reserve from Worldview-3 imagery. *Remote Sens.* 8(1): 24. <https://doi.org/10.3390/rs8010024>

Yu, X., Hyyppä, J., Litkey, P., Kaartinen, H., Vastaranta, M., Holopainen, M., 2017: Single-sensor solution to tree species classification using multispectral airborne laser scanning. *Remote Sens.* 9(2): 108. <https://doi.org/10.3390/rs9020108>

Zhang, B., Zhao, L., Zhang, X., 2020: Three-dimensional convolutional neural network model for tree species classification using airborne hyperspectral images. *Remote Sens. Environ.* 247: 111938. <https://doi.org/10.1016/j.rse.2020.111938>

Zhang, Z., Kazakova, A., Moskal, L.M., Styers, D.M., 2016: Object-based tree species classification in urban ecosystems using LiDAR and hyperspectral data. *Forests* 7(6): 122. <https://doi.org/10.3390/f7060122>

Zhou, J.H., Zhou, Y.F., Mu, W.S., 2011: Mathematic descriptor for identifying plant species: A case study on urban landscape vegetation. *J. Remote Sens.* 15(3): 524–538.



© 2026 by the authors. Submitted for possible open access publication under the terms and conditions of the Creative Commons Attribution (CC BY) license (<http://creativecommons.org/licenses/by/4.0/>).

Received: June 27, 2024  
Accepted: September 28, 2025

---

Author's address:

Huaipeng Liu, PhD \*  
e-mail: [gatestudy@163.com](mailto:gatestudy@163.com)  
Luoyang Normal University  
School of Geography and Tourism  
Henan Province  
471934, Luoyang  
CHINA